# Five-leg transformer model for GIC studies

Nicola Chiesa, Abbas Lotfi, Hans K. Høidalen, Bruce Mork, Øyvind Rui, Trond Ohnstad

***Abstract*—Geomagnetic induced currents (GIC) may saturate transformer cores and lead to increased reactive power consumption and disoperation of power systems. The paper analyses the influence of transformer core topology and the air-path inductances on the GIC response. Air-paths inductances are calculated with finite element method and are shown to be much larger for DC than for 50 Hz. Air-path inductances play a significant role for reactive power consumption and differential currents due to the deep saturation of the outer limbs of the 5-legged transformer. The paper analyzes reactive power consumption and differential current harmonics related to power system protection.**

***Keywords*: Transformer Modeling, GIC, Duality Transformation, Hybrid Model, Zero Sequence Flux, FEM**

## I. Introduction

Geomagnetically induced currents (GICs) are an effect of solar storm and induced geomagnetic disturbances on the power networks. Charged particles coming from the sun interact with Earth's magnetosphere-ionosphere and produce ionosphere currents that perturb Earth's geomagnetic field, inducing an Earth's surface potential gradients (3-6 V/km). The voltage difference between two grounding points results in the flow of zero-sequence currents called GIC [1,2]. The frequencies of these currents are very low and can be considered as quasi-DC. The duration of these incidents can be in the order of several minutes to several hours [1,3].

A DC current flowing through the windings of a power transformers generates a DC flux in the core with a magnitude depending on the magnitude of the DC current, number of turns in the windings carrying the current and reluctance of the DC flux path. This impressed DC flux shifts the operating point of the magnetizing characteristic and causes half cycle saturation in the core resulting in harmonic currents, forcing the flux to flow outside the core and increased reactive power consumption [4,5].

The important aspects to consider for analyzing a DC biased power transformer are the topology of the core, the nonlinearity of ferromagnetic materials, the coupling and connection of coils, and the system series resistances.

The GIC phenomenon is analyzed in several papers for both single- and three-phase transformers. These include FEM-based models [6,7], and magnetic circuit models [8-14]. The FEM models can be very accurate particularly for the cases where power losses and temperature rises in the tank and other metallic components are of interest. However, the requirement of detailed design information and the computational burden makes the application of FEM modeling not viable for power system studies.

The models based on magnetic circuit theory have been widely used for the analysis of GIC effects on transformers. Some models consider only very basic magnetic circuits lacking a topological representation of the core structure and DC flux paths, and using only simple calculation of model parameters [8,9]. More advanced models proposed for GIC studies are based on a topologically correct core representation modeling independent core sections and air-flux paths [10-15]. In particular, [2] analyses a 5-legged transformer topology and saturation of core elements. However, two main issues are not considered in these models. The first issue is the role of air-path reluctances on the flux distribution in different flux paths. The second one is the investigation of DC flux offset effect on the amplitude and harmonic content of the magnetizing current, as well as on reactive power consumption.

DC flux impressed in the windings is in the same direction for all legs, therefore the flux will flow through the zero sequence flux (ZSF) path. In the case of three-phase three-leg constructions, the ZSF goes outside the core, flows through the air gap and tank and returns to the core. For five-leg constructions, the lateral legs act as return paths for ZSF. As long as they do not saturate, the air-paths and the tank will have no considerable effect. For high level of GIC the lateral legs saturate and part of the flux flows outside the core through the oil and the tank leading to increased losses and the temperature rise in the tank.

This paper contributes with a modeling approach for the analysis of the effect of GIC in power transformers with focus on air-path inductances estimation and sensitivity, harmonic content of the magnetizing current, reactive power consumption and GIC influence on protection relays. Section II describes the transformer test object and modeling of the associated source and loads, as well as the GIC excitation. Section III describes calculation of air-path inductances based on a finite element approach. Section IV shows calculation results of internal fluxes, power consumption, and current harmonics. Section V discusses the results with respect to relay protection and application of the modeling approach to three-limb transformers.

N. Chiesa is with Sintef Energy Research, Norway, (Nicola.Chiesa@sintef.no)
A. Lotfi and H. Kr. Høidalen are with Norwegian University of Science and Technology (NTNU), Electric Power Engineering Department, N-7034 Trondheim, Norway, (abbas.lotfi@ntnu.no).
B. Mork is with Michigan Technological University (MTU), Houghton, Michigan, USA (bamork@mtu.edu).
Ø. Rui and T. Ohnstad. are with Statnett, Trondheim, Norway
This work was supported in part by the KMB project " Electromagnetic transients in future power systems" financed by the Research Council of Norway and by Dong Energy, EdF, EirGrid, Hafslund, National Grid, Nexans, RTE, Siemens WP, Statnett, Statkraft, and Vestas WS.

Paper submitted to the International Conference on Power Systems Transients (IPST2013) in Vancouver, Canada July 18-20, 2013.

## II. Modeling of GIC in Transformers

Fig. 1 shows the system topology considered for the analysis of GIC. Table I gives the rating and design information of the 300 MVA five-limb power transformer used in this study. The transformer has been modeled using the Hybrid transformer model approach [16,17]. No-load test report up to 115% excitation was available, as well as additional test and design data useful for parameter estimations and for the FEM modeling presented in Section III. The air-core inductance of HV winding is estimated to be 2.22 pu of leakage inductance between high- and low-voltage winding. An accurate estimation of air-core inductance is essential for GIC studies due to the high saturation regime.

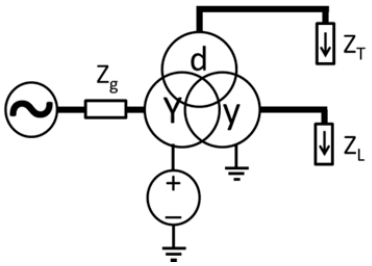


Fig. 1: System topology.

TABLE I
Transformer Rating and Design

| | | | |
|---|---|---|---|
| HV | 300 kV | 300 MVA | YN |
| LV | 132 kV | 300 MVA | yn0 |
| TV | 47 kV | 100 MVA | d11 |
| $A_{YOKE}/A_{LEG}$=0.6 | | $L_{YOKE}/L_{LEG}$=2 | |
| $A_{OUTER}/A_{LEG}$=0.6 | | $L_{OUTER}/L_{LEG}$=2.25 | |

Fig. 2 shows the equivalent electrical circuit of a 5-legged transformer core (excluding losses). This is similar to what is used in the Hybrid Transformer model [16] except for the additional air-path inductances $L_{air}$.

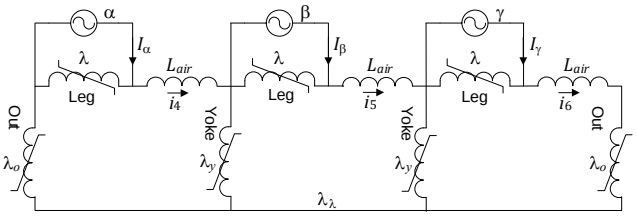


Fig. 2: 5-legged transformer core electric topology.

The transformer is loaded at 73% with $Z_L = 100+j\omega 10^{-4}\ \Omega$ on secondary and $Z_T = 50\ \Omega$ on tertiary winding. $Z_g$ is a negligible resistive series source impedance of 20 mΩ.

The representation of GIC in EMT studies is obtained by imposing a DC voltage offset on the HV neutral point. To avoid a step excitation and to resemble the longsome nature of GIC, the DC voltage is applied with a slow ramp between 2 and 10 s. A direct injection of a DC current on the neutral point is not suitable as this would not allow any flow of current harmonics. The value of the DC voltage offset and the series resistance determine the amplitude of GIC:

$$GIC = \frac{V_{DC}}{\mathrm{Re}(Z_g)+R_W} \quad (1)$$

with $R_W$ the HV winding resistance. The reference to the GIC amplitude instead of the DC voltage offset makes the analysis of GIC more convenient as the value of $Z_g$ does not influence the results.

Equation (1) is derived by the saturation equilibrium condition [2]:

- a quasi-DC earth-surface voltage establish a DC core flux offset;
- the flux offset drives the transformer into saturation leading to the flow of unidirectional current pulses;
- the DC component of current pulses generates a DC voltage drop on the system series resistances;
- the flux offset continues to increase at a decreasing rate until the voltage drop equals the DC earth-surface voltage eliminating the DC voltage applied to the transformer;
- when this equilibrium is reached the half-cycle saturation reaches a steady-state condition as long as the DC source is present.

The saturation equilibrium is demonstrated in Fig. 3 and Fig. 4 where the system of Fig. 1 is simulated with DC neutral voltage applied and no AC source. These figures have a conceptual meaning only as superposition of the AC and DC fluxes is not valid for a nonlinear system. The lack of air-paths and the homopolar flux in the transformer leg, impose a fixed flux ratio of 0.5 in the yoke and of 1.5 in the outer-limbs. A reduced cross-section area of the yokes and outer-limbs results into a high flux density, leading first the outer-limbs in saturation.

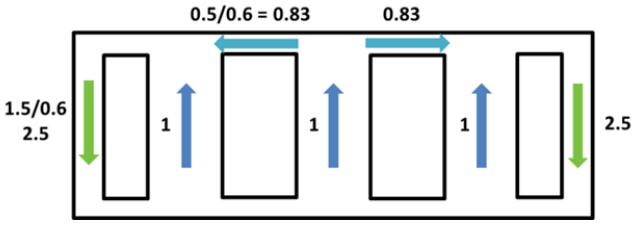


Fig. 3: Flux distribution in zero-sequence excitation without air-paths, with indication of relative flux densities.

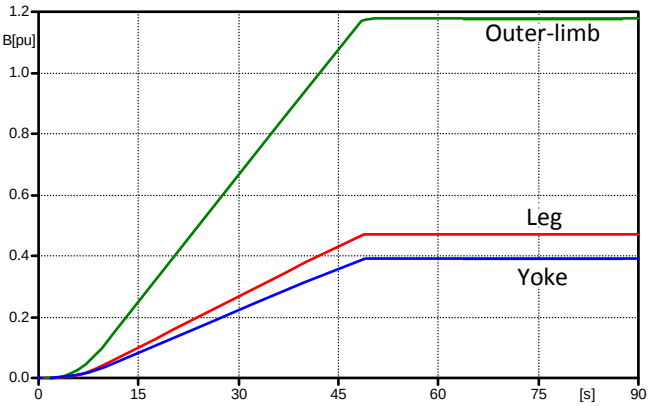


Fig. 4: Per unit magnetic field in different core sections with neutral voltage applied according to Fig. 1 without any air-path inductances and AC source applied.

The effect of the air-path across each leg is considered in

Fig. 5 and Fig. 6. Flux starts flowing into air-paths only after the outer-limb are fully saturated (in Fig. 6 after 46s). The effect seen in Fig. 6 is that the flux density reached in the legs at saturation equilibrium is higher than in the case without air-paths. This results in different relative flux density distribution in the core as indicated in Fig. 5.

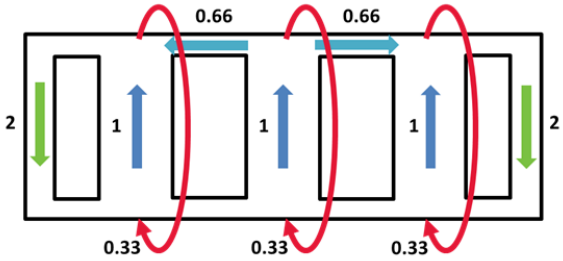


Fig. 5: Flux distribution in zero-sequence excitation including air-paths, with indication of relative flux densities at saturation equilibrium.

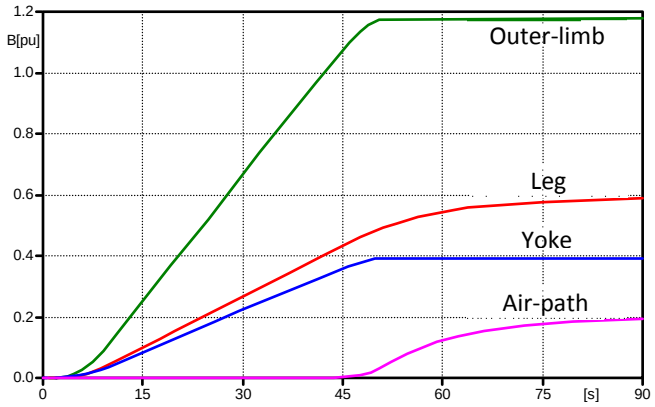


Fig. 6: Per unit magnetic field in different core sections with neutral voltage applied according to Fig. 1 with air-path inductances added (500 mH), but without AC source applied.

## III. Air Path Inductance Calculation

In order to quantify air-path inductance values, 3D-FEM calculations are performed for the transformer in Table I. Fig. 7 shows this transformer modeled in ANSOFT MAXWELL. Design details for winding, core, and tank were available but this cannot be brought here. Extended zero-sequence tests were also available. Because of symmetry, only half of the transformer is modeled as this dramatically decreases solving time and memory requirements. The innermost winding of the transformer is the low voltage winding (132 kV), the next are high voltage winding (300 kV), and tertiary winding (47 kV), respectively.

Running the FEM software in Eddy current and Magneto-static mode and using the energy method, the inductance matrix is calculated. The short-circuit zero-sequence impedances (SCZSI) at different cases corresponding to the tests done on this transformer are calculated, for the purpose of verifying the FEM model.

Table II shows the SCZSI obtained by 3D-FEM simulation compared with the test results. The obtained values illustrate good agreement between the test results and FEM calculations. Tap numbers 13, 1 and 25 refer to principal, maximum and minimum taps, respectively.

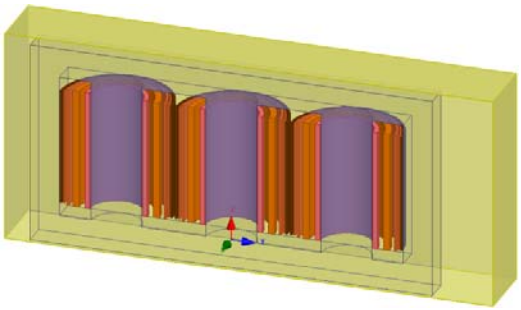

Fig. 7: 3D-model of the case study.

TABLE II
Calculated and Measured Values of ZSI

| Windings Excited/shorted | Tap | Meas-ured | 3D-FEM | Error % |
|---|---|---|---|---|
| HV300kV/TW47kV | 13 | 107,2 | 105.18 | 1.88 |
| HV300kV/TW47kV | 1 | 116.8 | 115.56 | 1.06 |
| HV300kV/TW47kV | 25 | 99.69 | 97.9 | 1.8 |
| LV132kV/TW47kV | - | 31.85 | 32.63 | -2.45 |

When GIC occurs, there is a DC flux in each leg that can cause the lateral legs to saturate. In this case the flux goes outside the core and returns via air (oil) gaps and the tank as shown in Fig. 8. The inductances corresponding to these paths appear in the core model shown in Fig. 2 obtained by duality transformation and is called $L_{air}$.

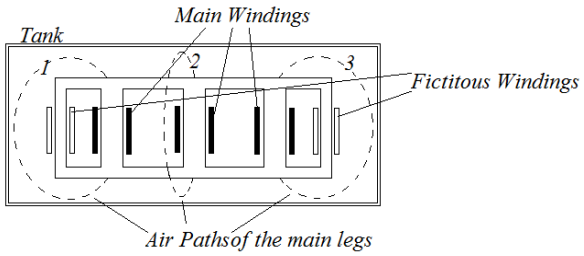


Fig. 8: Flux Paths outside the core

The air paths inductances cannot be obtained from typical zero-sequence tests, because the measured inductances are associated with the combination of the lateral leg in parallel to the relevant air-path. These cannot be separated from each other for moderate excitations. In the case of FEM modeling, the flux can be forced to go outside the core by placing two fictitious windings on the lateral legs as shown in Fig. 8. Applying the same exciting current to the mentioned windings and calculating the inductance matrix, the voltage of each winding will be:

$$V_i = j\omega \sum_{k=1}^{5} L_{ki} I_k,\ i = 1 \dots 5 \quad (2)$$

The currents are the same, so:

$$V_i = I_p \cdot (j\omega \sum_{k=1}^{5} L_{ki}),\ I_k = I_p, k = 1 \dots 5 \quad (3)$$

This results in:

$$L_{air,i} = \frac{V_i}{I_p} \rightarrow L_{air,i} = \sum_{k=1}^{5} L_{ki} \quad (4)$$

The air–paths shown in Fig. 8 also involve the tank. Thus

$L_{air,i}$ is the sum of the air-gap and tank inductance. Since the penetration depth of magnetic flux in tank decreases with frequency, the equivalent reluctance of tank increases leading to a decrease of the corresponding inductance. For the transformer modeled in this paper values of these inductances are as shown in Table III. The inductances values are referred to the innermost LV winding. As can be seen in table III, this decrease in the inductance caused by magnetic penetration depth is considerable even at 50 Hz excitation.

TABLE III
AIR-PATH INDUCTANCES CALCULATED BY 3D-FEM

| Inductance corresponding to the air-path of Fig.8 (mH) | DC Excitation | AC Excitation, 50 Hz |
|---|---|---|
| 1, 3 | 736.65 | 225.895 |
| 2 | 771.99 | 242.593 |

The corresponding inductances are not voltage dependent for expected amp-turns generated by GIC phenomenon since the reluctance of the air-paths dramatically dominate the iron sections (leg and the tank). In other words, it is not expected that the tank walls, cover and bottom will be heavily saturated. However, the magnetic penetration depth in the tank makes the air-path inductances frequency dependent. If a detailed investigation of the flux outside the core is of interest, the inductance $L_{air}$ should be considered as a frequency dependent parameter. In this case the tank losses can be taken into account for instance as a resistive element in combination with inductive branches in a Cauer circuit.

For the purpose of this paper we consider an average, frequency-independent value for investigating the effect of the $L_{air}$ on terminal quantities.

## IV. RESULTS

The system of Fig. 1 is simulated with different level of GIC from 20 to 500 A and different values of air-path inductance. The base reference case is for 100 A GIC and 500 mH/phase air-path inductances.

Fig. 9 shows the increased reactive power consumption as a well-known effect of GIC. For this specific transformer a 100 A GIC results in an increased 36 MVAr reactive power demand. Since GIC is a system-wide phenomenon affecting several transformers simultaneously, power utilities are particularly concerned about extraordinary reactive power demand due to voltage stability concerns and reactive power reserve scheduling.

Table IV compares the simulation results at steady-state (no GIC) with the case of 100 A GIC for different values of air-path inductance. While there is a minor effect of the GIC on active power and terminal RMS current, the reactive power increases by a factor of 3 for the analyzed system configuration. Not considering the air-path inductance has a considerable effect on the increased reactive power demand ($\Delta Q = Q_{GIC} - Q_{SS}$) with difference in the order of 10-20% underestimation for this transformer. On Fig. 10 the reactive power $Q$ is shown to be directly proportional to GIC.

$Q$ is calculated here using the traditional definition of reactive power $\sqrt{S^2 - P^2}$ at saturation equilibrium; however, under distorted conditions this definition includes harmonic reactive power components. Since only fundamental lagging current components have a significant impact on system voltage profile [15], the fundamental reactive power is defined as:

$$Q_{50Hz} = \sqrt{3V^2 I_{50Hz}^2 - P^2} \tag{5}$$

with $I_{50Hz}$ being the fundamental harmonic of the current and assuming that the voltage has no harmonic distortion.

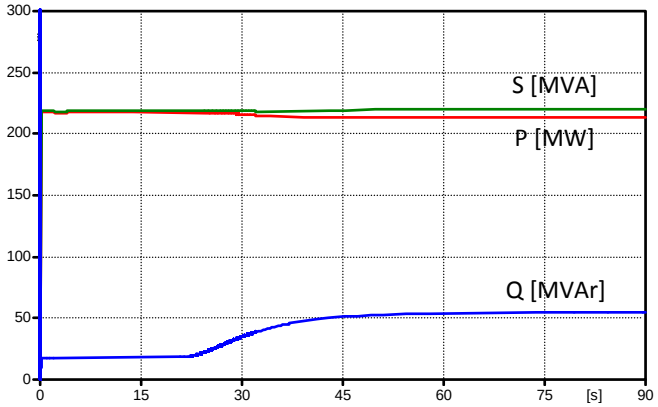

Fig. 9: S, P and Q variation due to GIC (100 A), with air-path inductances (500 mH).

TABLE IV
POWER AND CURRENT INTO TRANSFORMER

| | Steady State | 100A GIC at Saturation Equilibrium | | | |
|---|---|---|---|---|---|
| | | Without air-path | 250 mH | 500mH | 750mH |
| S [MVA] | 219 | 219 | 219 | 220 | 220 |
| P [MW] | 218 | 214 | 213 | 213 | 213 |
| Q [MVAr] | 18 | 47 | 52 | 54 | 56 |
| ΔQ [MVAr] | - | 29 | 34 | 36 | 38 |
| *$Q_{50Hz}$ [MVAr]* | *8* | *36* | *39* | *40* | *41* |
| Irms [A] | 419 | 421 | 422 | 423 | 424 |

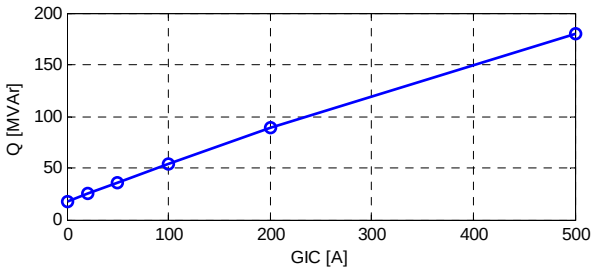

Fig. 10: Reactive power consumption as function of GIC.

Fig. 11 and Fig. 12 are the extension of Fig. 4 and Fig. 6, respectively, with both AC source and neutral voltage applied according to Fig. 1. It is harder to read these figures compared to Fig. 4 and 6, but we can observe the same behavior with a DC flux offset in leg, yoke and outer-limb. The magnitude of outer-limb flux is reduced once saturated, and the top of the positive peak is limited due to the unidirectional saturation.

Air-path inductance effect is noticeable only once the outer-limb becomes fully saturated and contains both a DC and AC components. Air-path inductance has only a minor effect on the magnitude of the leg fluxes.

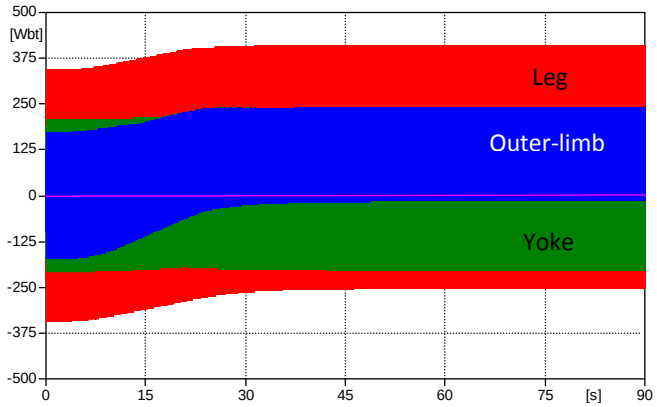


Fig. 11: Flux-linkages in different core sections with AC source and neutral voltage applied (100 A GIC) according to Fig. 1 without any air-path inductances.

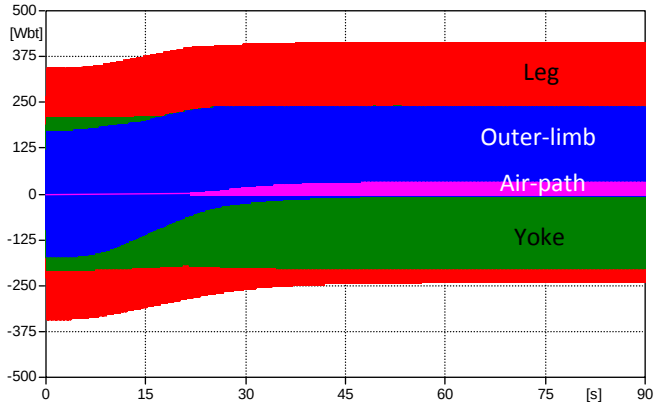


Fig. 12: Flux-linkages in different core sections with AC source and neutral voltage applied (100 A GIC) according to Fig. 1 with air-path inductances added (500 mH).

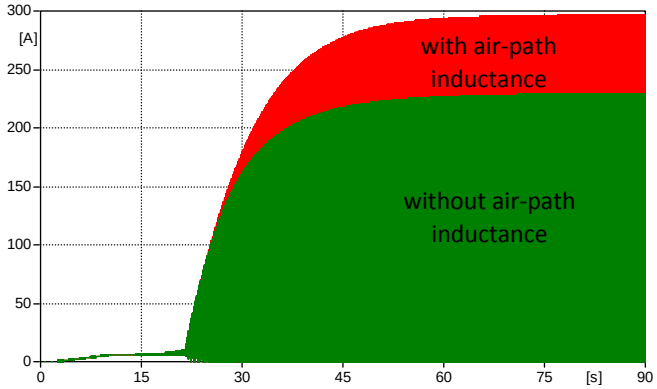


Fig. 13: Transformer differential phase current, with (500mH) versus without air-path representation for 100 A GIC.

Fig. 13 shows that the influence of the air-path inductances on the differential current is significant. For the same GIC current (same DC component) Fig. 14 and Fig. 15 show a considerable difference in the harmonic content of the transformer differential current. In case of GIC, the differential current is a direct effect of the core saturation and increased distorted magnetization current and flows in the neutral of the transformer.

The harmonic analysis of the differential current in Fig. 15 shows the presence of all even and odd harmonics typical of unidirectional waveforms and similar to those typically found in transformer inrush currents.

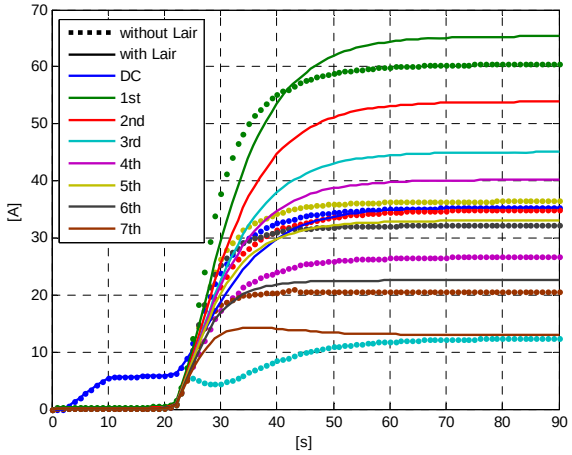


Fig. 14: Evolution of harmonic content of differential phase current, without and with (500mH) air-path inductances for 100 A GIC.

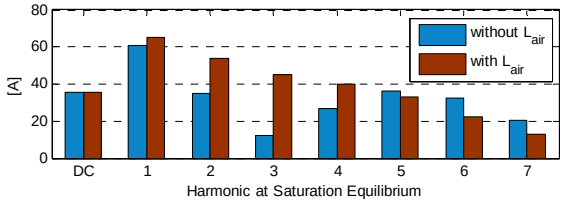


Fig. 15: Harmonic content of differential phase current at saturation equilibrium, without and with (500mH) air-path inductances for 100 A GIC.

## V. Discussion

In addition to the increased reactive power demands, power utilities are concerned with the protection relay false tripping due to GIC. Relevant protection schemes that may be affected by GIC are differential protection and high-impedance ground-fault protection installed on HV side.

How the GIC will influence the protection of the transformer is a complex issue. To get a clear answer saturation of the current transformers should be taken into account in the simulations and the simulated waveforms should be applied to a real protection relay.

Generally, the differential protection of the transformer is set for clearing internal short circuits or external short circuits close to the transformer. Differential protections have harmonic stabilization normally on the $2^{nd}$ and $5^{th}$ harmonics. $2^{nd}$ harmonic stabilization may be only active at transformer energization. For higher values of these harmonics the trip is blocked. A typical relay characteristic with harmonic traces as function of the GIC is shown in Fig. 16. Different level of GIC gives equivalent harmonic curves with the tip function of the GIC level. In Fig. 16, only unusual high level of GIC may

trigger the differential protection. However, protections may still trigger as a result of saturation in the current transformers. The system-wide protection response to GIC should be further investigated.

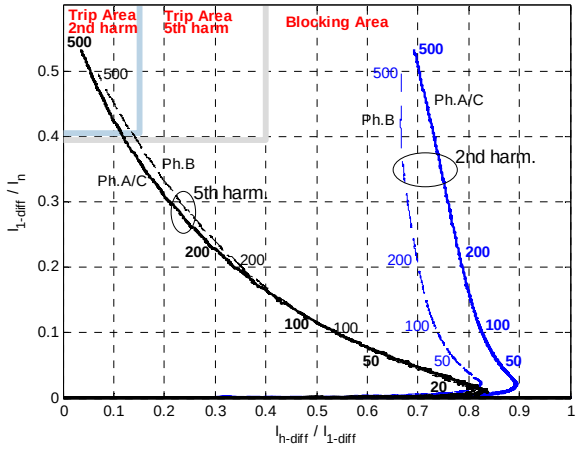


Fig. 16: Differential current protection: 2nd and 5th harmonics blocking characteristics. Harmonic traces as function of the GIC numbered in Ampere along the curves for phases A/C and B.

The modeling approach and air-path inductance estimation method presented in this paper can be applied to three-limb transformers. Three-limb transformers do not have an iron zero-sequence path, therefore only the air-paths determine the response of GIC and should be estimated with great accuracy. Nevertheless, three-limb transformers have the advantage that air-path inductances can be measured from open-circuit zero-sequence tests.

## VI. Conclusions

The GIC response is shown to be significantly affected by the air-path inductances even in five-limb cores. Transformer models used for the investigation of GIC phenomenon should have at least the following characteristics:

- topology correct core representation;
- accurate representation of highly saturated state by taking into account the air-core inductance;
- modeling of the flux paths outside by air-path inductances.

The most critical core sections are the outer-limbs as they become highly saturated in the event of GIC. The ratio between the fully saturated outer-limb inductance and the air-path inductances determines the extent of flux forced outside the core. FEM seems to be the only viable alternative for the calculation of air-path inductances in five-limb transformers. When relevant, transformer manufacturers should be able to provide the value of air-path inductance, and empirical methods for the estimation of this parameter should be developed as FEM modeling is inconvenient in most circumstances.

The accurate transformer model presented in this paper is an important basis for further work on protection response.

## VII. Aknowledgments

The authors wish to thank ABB Ludvika and Hafslund Nett for providing access to transformer data.

## VIII. References

[1] P. Price, “Geomagnetically induced current effects on transformers,” *Power Delivery, IEEE Transactions on,* vol. 17, no. 4, pp. 1002-1008, 2002.

[2] Walling, R. A.; Khan, A. N. “Characteristics of transformer exciting-current during geomagnetic disturbances*”, IEEE Transactions on Power Delivery*, Vol. 6,_Issue: 4, pp. 1707-1714, 1991.

[3] R. Pirjola, “Geomagnetically induced currents during magnetic storms,” *IEEE Trans. Plasma Sci.*, vol. 28, no. 6, pp. 1867–1873, Dec. 2000.

[4] Kappenman J.G.: ‘Transformer dc excitation field test and results’. IEEE PES Special Panel Session Report, 90 TH0291-5 PWR, 12 July 1989

[5] Kappenman J.G., ALBERTSON V.D., MOHAN N.: ‘Current transformer and relay performance in the presence of geomagnetically-induced currents’, IEEE Trans. Power Appar. Syst., 1981, 3, (PAS-100), pp. 1078–1088

[6] B. Zhang, L. Liu, Y. Liu, M. McVey and R. Gardner, “Effect of geomagnetically induced current on the loss of transformer tank,” *Electric Power Applications, IET,* vol. 4, no. 5, pp. 373-379, 2010

[7] Seyed Ali Mousavi, “lectromagnetic Modelling of Power Transformers with DC Magnetization”, Licentiate Thesis in Electromagnetic Engineering, TRITA-EE 2012:057, ISBN 978-91-7501-537-8, Royal Institute of Technology (KTH), , Stockholm, Sweden 2012

[8] Xuzhu Dong; Yilu Liu; Kappenman, J.G., “Comparative Analysis of Exciting Current Harmonics and Reactive Power Consumption from GIC Saturated Transformers”, Power Engineering Society Winter Meeting, pp. 318 – 322, vol.1, 2001

[9] Jinxia Yao; Min Liu; Changyun Li; Qingmin Li, “Harmonics and Reactive Power of Power Transformers with DC Bias” Power and Energy Engineering Conference (APPEEC), 2010 Asia-Pacific, Pp. 1–4, 2010

[10] Hongzhi Li; Xiang Cui; Tiebing Lu; Zhiguang Cheng; Dongsheng Liu, “An improved magnetic circuit model of powertransformers under DC b ias excitation”, Electromagnetic Compatibility (APEMC), 2010 Asia-Pacific Symposium on, pp. 806 – 809, 2010

[11] Masoum, Mohammad A.S.; Moses, Paul S., “Influence of Geomagnetically Induced Currents on three-phase power transformers”, Power Engineering Conference, 2008. AUPEC '08. Australasian Universities, pp. 1–5, 2008

[12] E. F. Fuchs, Y. You, and D. J. Roesler, "Modeling and simulation, and their validation of three-phase transformers with three legs under DC bias," *IEEE Transactions on Power Delivery*, vol. 14, pp. 443-449, 1999.

[13] E. F. Fuchs and Y. Yiming, "Measurement of Lambda-I characteristics of asymmetric three-phase transformers and their applications," *IEEE Transactions on Power Delivery*, vol. 17, pp. 983-990, 2002.

[14] D. Tousignant, L. Bolduc, A. Dutil, “A method for the indication of power transformer saturation”, Electric Power Systems Research, Volume 37, Issue 2, May 1996, Pages 115–120

[15] Picher, P.; Bolduc, L.; Olivier, G., “Acceptable direct current in three-phase power transformers: comparative analysis”, Electrical and Computer Engineering, 1997. Engineering Innovation: Voyage of Discovery. IEEE 1997 Canadian Conference on, pp. 157-160 vol.1, 1997

[16] H. K. Høidalen, B. A. Mork, F. Gonzalez, D. Ishchenko, N. Chiesa: “Implementation and verification of the Hybrid Transformer model in ATPDraw”, *Electric Power Systems Research* 79 (2009), 454-459.

[17] Mork, B.A.; Ishchenko, D.; Gonzalez, F.; Cho, S.D.: "Parameter Estimation Methods for Five-Limb Magnetic Core Model", IEEE Transactions on Power Delivery, Vol. 23 , pp. 2025-2032, 2008.